Cavity-Enhanced Absorption Detection of H₂S in the Near Infrared Using a Gain-switched Frequency Comb Laser

S. Chandran[1], S. Mahon[1,#], A.A. Ruth[1,*], J. Braddell[2], M.D. Gutiérrez[2]

[1]*Physics Department & Environmental Research Institute, University College Cork, Cork, Ireland*

[2] *Pilot Photonics Limited, Invent Centre, Dublin City University, Glasnevin, Dublin 9, Ireland*

Abstract

A custom-designed gain-switched frequency comb laser was passively coupled of to a medium finesse cavity in the region between 6346 cm^{-1} and 6354 cm^{-1} for the development of a prototype cavity enhanced absorption setup. The setup was applied to static gas detection of hydrogen sulfide at the parts per thousand level in a laboratory environment. A Fourier transform spectrometer was used for signal detection. The experimental performance of the setup was characterized in this proof-of-principle investigation; advantages, drawbacks and future scope of the approach are discussed in this article.

*Corresponding Author. Email: a.ruth@ucc.ie, Tel: +353-21-4902057, Fax: +353-21-4276949

#Current address: Scottish Microelectronics Centre, King's Buildings, Alexander Crum Brown Road, Edinburgh EH9 3FF, United Kingdom

28

1.   Introduction

Among the many applications of frequency combs (FC) in metrology (e.g. optical clocks and low noise frequency synthesis) [1-3], combs have long been recognized as superior light sources for absorption spectroscopy [4-6]. FC lasers generate a large stable array of equally spaced, phase-coherent, narrow-band spectral lines. In excess of 10^5 comb lines can be produced with mode-locked short pulse lasers, with line spacing in the region of many 10s of MHz (depending on the comb laser's repetition rate [1]). The comb lines' narrow bandwidth is determined by the coherence time of the laser.

In many cases the spectral resolution in absorption experiments is however limited by the spectrometer used for detection. In these cases FCs are essentially broadband lasers which act as a "spectral ruler" [1]. To exploit the inherently high resolution of FCs, new detection schemes using virtually imaged phase arrays spectrometers [7-9], comb-cavity vernier approaches [10,11] and Fourier-transform based dual comb spectroscopy [12-17] have been established. Some of these methods were recently reviewed [18]. To enhance the sensitivity in absorption experiments, applications of FCs in conjunction with optically stable cavities covering a spectral range that is limited by the high reflectivity range of the cavity mirrors have been developed [19,20]. The key challenge of cavity-enhanced FC absorption spectroscopy is the coupling of the FC to the cavity by matching the comb lines to an appropriately designed mode structure of a high finesse cavity – different approaches to coupling and locking of FC lines to high finesse optical cavities have also been reviewed [21].

In contrast to developing ultimate instrumental limits, the approach to cavity-enhanced absorption detection in this work aims at experimental simplicity. The principle suitability of a custom-built gain-switched frequency comb (GSFC) laser in conjunction with a very modest optical cavity was examined without spectrally stabilizing or mode-matching the cavity. GSFCs are tunable FCs that are simple in design and significantly cheaper than mode locked femtosecond FC lasers [22]. They, however, do not deliver the finely spaced large number of comb lines and span a significantly smaller wavelength region (~typically a few nm). GSFCs are generated by the direct modulation of commercially available laser diodes, as a distributed feedback laser, with a radiofrequency (RF) sine wave. External optical injection in a master-slave laser configuration can be employed to generate narrow line widths and low intensity noise [23]. GSFCs can also be integrated as a

59   monolithic devices [24] (see conclusion & outlook). The approach is simple and cost-efficient,

60   and enables wavelength tunability of the comb and the line spacing, but with a rather limited

61   number of comb lines [22]. GSFC lasers are commonly used as benchtop units for optical

62   telecommunication in the C-band [22]. Recently a dual comb GSFC setup was reported based on

63   gain switching and optical injection locking [25], with potential applications of the dual comb

64   architecture in the mid-IR or near UV. In Ref [25] the absorption feature of $H^{13}CN$ in the 1.5 μm

65   region were reported.

66   The objective of this study was to simply tune more than one laser comb line to absorption features

67   of an appropriate target gas (hydrogen sulfide, H_2S) and to achieve sensitivities below the

68   combustion limit of the hazardous gas in the parts per thousand (ppTv) regime using a low finesse

69   ($f \sim 450$) optical cavity without a mode matching schemes.

70
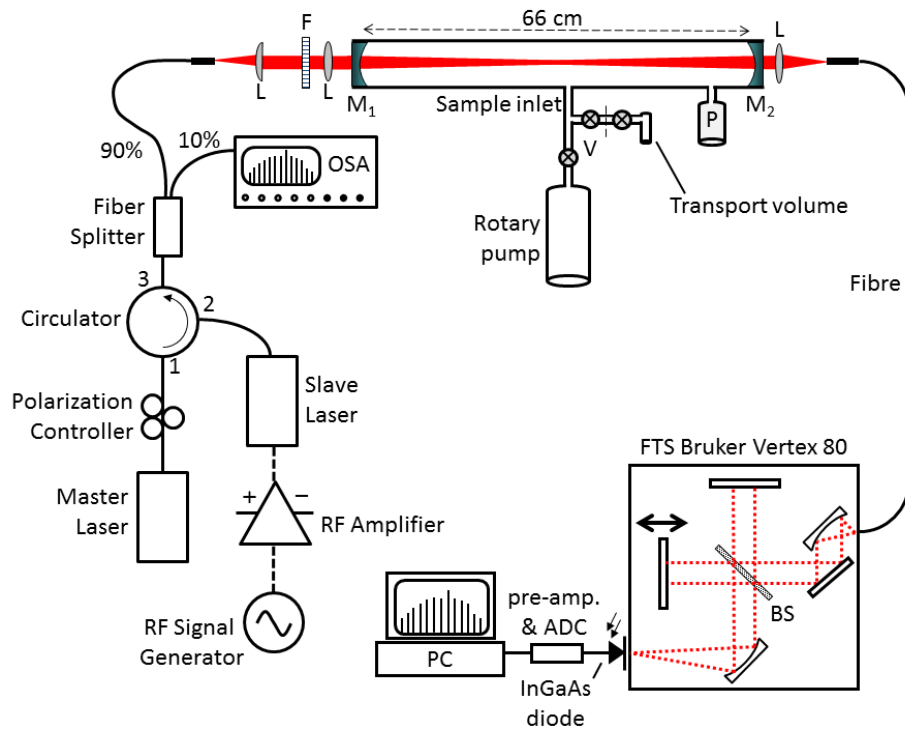
71   **Fig. 1** Schematic of the experimental setup. Mirrors M_1 and M_2 are high-reflectivity dielectric mirrors ($R\sim0.993$)
72   forming a medium finesse optical cavity with a length of 66 cm. L: Lenses used for collimation and light collection.
73   P: Absolute Pressure gauge. V: Valves. RF: Radio Frequency (~10 GHz). ADC: Analog-to-Digital Converter. OSA:
74   Optical Spectrum Analyzer.

75

76

77

3

78 **2.   Experiment**

79   The schematic of the experimental setup is shown in Fig. 1. The main components of the GSFC

80   laser were a tunable master laser (HP-8168F), a distributed feedback slave laser (Thorlabs, ITC-

81   502), an radio frequency (RF) signal generator (HP-83751A), a biased RF amplifier (Aldetec,

82   ALP-0618S430), a polarization controller, and a circulator. The slave laser was kept at a stable

83   operating temperature by employing a thermoelectric cooler and a thermistor in the laser package.

84   The (tunable) frequency of the master laser was slightly detuned (to higher energies) from that of

85   the slave laser. Polarization controlled light from the master laser was injected via a circulator

86   (ports 1 & 2) into the slave laser. The optical injection power was ≈3.1 mW (5 dBm). For a DC

87   bias current of 45.1 mA the gain switching was achieved by continuously driving the slave laser

88   above and below its laser threshold using an amplified sinusoidal RF signal. This created a train

89   of pulses corresponding to an optical comb in the frequency domain. The (tunable) frequency of

90   the RF generator hence determined the free spectral range of the FC, which in the present

91   experiment was typically maintained at ~10 GHz (see Fig. 3). The absolute center frequency of

92   the GSFC was controlled through the frequency of the master laser, which was tunable external

93   cavity diode laser. In this experiment wavelength of the master laser was typically maintained at

94   ~1574.8 nm (~6349.4 cm^{-1}); cp. Fig. 3. Overall the GSFC produced twenty phase-coherent,

95   equally spaced comb lines with an individual spectral width of ~300 kHz [23] covering a range

96   from 6346 to 6354 cm^{-1} (1575.8…1573.8 nm) in the near infra-red with an overall quasi-

97   continuous integrated power close to ≈4 mW (6 dBm). For monitoring the GSFC emerging from

98   port 3 of the circulator (Fig. 1), the light was split into two beams (ratio 90:10) and the less intense

99   fraction of the beam was guided to an optical spectrum analyzer (OSA, Advantest Q8384). The

100   main beam (90%) was collimated with a plano-convex (f ~ 25 mm) and a biconvex lens (f ~ 75

101   mm). The collimated light was guided into a stable optical cavity consisting of two plano-concave

102   dielectric mirrors (diameter 25 mm, $r = -200$ cm, Layertec GmbH) at a distance of $d = 66.0\pm0.1$

103   cm. The modest reflectivity of the cavity mirrors of $R = 0.993\pm0.001$ was measured with a double-

104   beam UV/Vis/NIR spectrometer (PerkinElmer, Lambda-1050). The optical cavity was enclosed

105   by a stainless steel vacuum tube (diameter ~ 40 mm) which was fitted with an access port for

106   evacuation and sample injection as schematically shown in Fig. 1. Before experiments the static

107   gas cavity was evacuated by a rotary pump to ~ 0.1 mbar. The light exiting the cavity was collected

108   with an achromatic lens and focused into a multimode light-guide (diameter 1.5 mm) which was

109   connected to the entrance aperture of a Fourier transform spectrometer (FTS, Vertex 80 with CaF_2

110   beam splitter, Bruker Ltd.). In the spectrometer an InGaAs photodiode was used to detect the light

111   transmitted by the cavity. Using the Bruker OPUS software spectra were recorded with a spectral

112   resolution of 0.08 cm^{-1} in an integration time of 120 s (corresponding to 4 scans per spectrum).

113   This integration time was based on the optimum measured signal-to-noise ratio of the FC,

114   established in a series of intensity stability measurements using the FTS and OSA.

115   Hydrogen sulfide (H_2S) (BOC Industrial Gases, >99.9%) was used as target gas in this proof-of-

116   principle experiment. It is a poisonous and corrosive gas that can occur as a pollutant in industrial

117   settings, such as oil refineries, production facilities involving petro-chemistry, gas processing

118   plants and gas fields. Since it is heavier than air it can accumulate in badly ventilated areas and

119   constitute a fire or explosion hazard due to its flammable nature [26]. The main source of H_2S as

120   a natural atmospheric pollutant is from volcanic activity. The changes in the H_2S release rate from

121   dormant volcanos in comparison to other trace species is used to monitor volcanic activity before

122   potential eruptions [26]. Thus the spectroscopic detection of H_2S in industrial and environmental

123   applications is of high relevance and motivated its usage in this GSFC application. High detection

124   sensitivity was however not expected a priori, due to the comparatively small absorption cross-

125   sections of H_2S in the spectral target region at ~6350 cm^{-1} and the modest mirror reflectivity.

126   **3.   Results and Discussion**

127   **3.1   Near IR overview spectrum of H_2S using FT-IBBCEAS**

128   Before matching frequency comb lines with absorption features of H_2S, its near IR spectrum was

129   measured in the region between 6000 and 6600 cm^{-1} using Fourier-transform incoherent broad-

130   band cavity enhanced absorption spectroscopy (FT-IBBCEAS) [27-29]. FT-IBBCEAS is an

131   approach to measure broadband cavity-enhanced spectra in the NIR region with high resolution

132   [30-32]. The spectrum was measured at a static H_2S pressure of ca. 3 mbar with an integration time

133   of 60 min and a spectral resolution of 0.08 cm^{-1} (cavity length 644 cm, mirror reflectivity $R \approx$

134   0.9998); for more details concerning the experimental setup see Ref [30]. The line positions

135   obtained agreed with those in HITRAN [33] and the Pacific Northwest National Laboratory

136   (PNNL) data base [34] to within the resolution of the instrument. Fig. 2 shows the overview

137   spectrum of the 2.5 polyad of H_2S (asymmetric top, point group C_{2v}) containing features of 5

138   combination overtone bands $\nu_1+3\nu_2$, $3\nu_2+\nu_3$, $2\nu_1+\nu_2$, $\nu_1+\nu_2+\nu_3$, and $\nu_2+2\nu_3$. The spectrum is subject

139   to resonance interactions between all states in this polyad. The same region was spectroscopically

140   studied previously by Ulenikov et al. [35]. The $\nu_1+\nu_2+\nu_3$ (asymmetric) and $2\nu_1+\nu_2$ (symmetric)

141   bands, centered at ~6289.17 cm^{-1} and ~6288.14 cm^{-1} exhibits, are the strongest combination bands

142   with clearly visible and overlapping P, Q and R ro-vibrational components; cf. Fig. 2. The bands

143    $\nu_1+3\nu_2$ and $3\nu_2+\nu_3$, are significantly weaker and especially the very weak combination overtone

144    $\nu_2+2\nu_3$ is negligible for detection applications. A transition in the R branch at ~6339.868 cm^{-1} was

145   used before by Modugno et al. [36] for detection of H$_2$S at the parts per million level (~4 ppmv)

146   using two-tone frequency modulation spectroscopy. More recently also Chen et al. [26] used R-

147   branch lines of $\nu_1+\nu_2+\nu_3$ at ~6362.88 cm^{-1} for off-axis integrated cavity output spectroscopy.

148
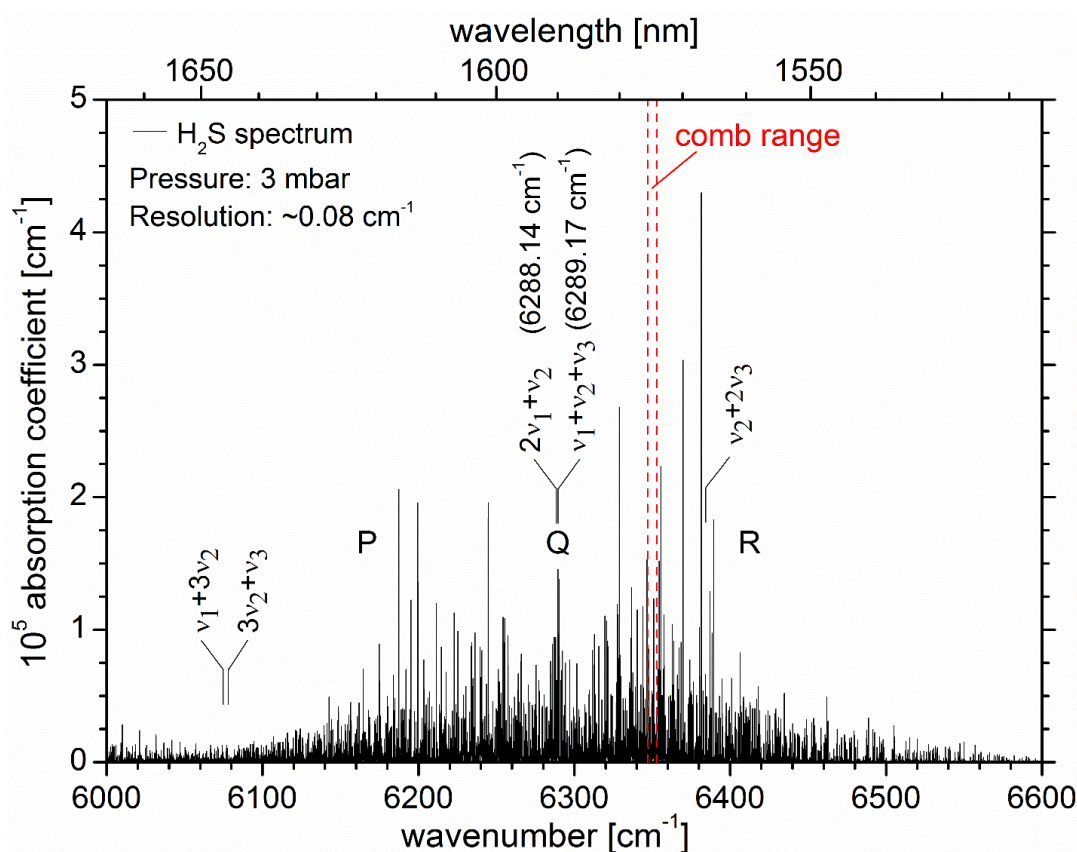
149   **Fig. 2** The near IR absorption spectrum of H$_2$S at 3 mbar recorded using FT-IBBCEAS with a resolution 0.08 cm^{-1}.
150   The region between 6000 and 6600 cm^{-1} is part of the v = 2.5 polyad. The two dashed vertical lines (red) in the R-
151   branch of the $\nu_1+\nu_2+\nu_3$ and $2\nu_1+\nu_2$ combination bands of H$_2$S indicate the spectral region where the GSFC (20 lines)
152   is located. Other band centers of weaker overtones in the region are also indicated.

153

154

155

156 **3.2   GSFC application to cavity-enhanced H₂S detection around 6350 cm⁻¹**

157   Owing to the limited tunability of the GSFC, ro-vibrational R-branch transitions of the $\nu_1+\nu_2+\nu_3$

158   combination band were used in this study to detect H_2S in the region around 6350 cm⁻¹, i.e. in the

159   spectral region indicated by two vertical red lines in Fig. 2. Matching comb lines with H_2S

160   absorption features turned out to be cumbersome as the FWHM of the absorption lines (as well as

161   the FC line widths) are smaller than the spectral resolution of the detection setup.

162   The HITRAN database [33] gives the H_2S FWHM self-broadening and air-broadening coefficients

163   at 296 K as ~0.316 cm⁻¹ atm⁻¹ and ~0.148 cm⁻¹ atm⁻¹, respectively (with negligible pressure shift).

164   Since the overview spectrum in Fig. 2 was measured at ~3 mbar of H_2S at room temperature,

165   pressure broadening was negligible (<0.001 cm⁻¹) and the expected FWHM due to Doppler

166   broadening at 296 K was $f_G \sim 0.013$ cm⁻¹. Thus the observed FWHM of the absorption lines in Fig.

167   2 were limited by the resolution of the FTS of 0.08 cm⁻¹.

168   The situation was similar for H_2S detection with the GSFC in the static gas, where the same FTS

169   was used in conjunction with the short optical cavity. The GSFC experiments were performed at

170   ~82 mbar total pressure where the expected FWHM of absorption lines due to pressure broadening

171   was $f_L \sim 0.012$ cm⁻¹ [33] (see also discussion below)[#1]. The value of f_L is approximately the same

172   size as the expected FWHM Doppler limit of 0.013 cm⁻¹ leading to an anticipated Voigt FWHM

173   of $f_V \approx 0.5346 f_L + \sqrt{0.2166 f_L^2 + f_G^2} = 0.021\,\text{cm}^{-1}$ [37]. Even though the comb lines possess a

174   small band width of only ≈10⁻⁵ cm⁻¹ [23], and even though the absolute comb position could be

175   finely tuned in relative steps of ~0.004 cm⁻¹, it was very cumbersome to overlap of comb lines

176   with H_2S absorption lines, because all cavity transmission spectra were measured with the limited

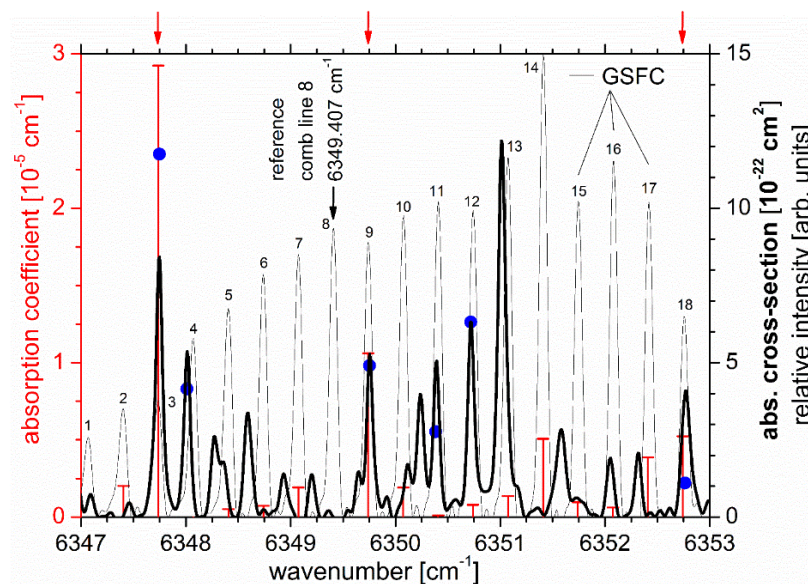177   spectral resolution of the FTS of 0.08 cm⁻¹ (i.e. approximately 3-4 times the FWHM of the

---

[#1]The true the mixing ratio in the cavity was 0.92 ppTv and hence the partial pressure of H_2S in the cavity was ca. 1 mbar (as will be shown below) and therefore the solely pressure broadened FWHM was expected to be

$$f_L(p) \approx \gamma_{\text{air}}\,(1\text{ atm})[\,p - p_{\text{self}}\,] + \gamma_{\text{self}}\,(1\text{ atm})\,p_{\text{self}} \approx 0.012\text{ cm}^{-1}. \tag{2}$$

based on HITRAN broadening coefficients mentioned in the text.

178   expected absorption lines).[#2] Therefore software was written that identifies the required FSR and

179   optimum GSFC center position (arbitrarily chosen as the position of line 8 – see Fig. 3) to match

180   as many comb lines as possible with absorption features in the relevant spectral region (see Fig.

181   2). In the software the GSFC spectrum was treated as a series of delta functions, owing to the small

182   bandwidth of $\approx 10^{-5}$ cm^{-1} (300 kHz) per comb line [23]. Using the measured H_2S spectrum in Fig.

183   2 the matching of up to three comb lines within experimental uncertainty was predicted for a center

184   position of 6349.4 cm^{-1} (position of comb line 8) and an FSR of 10 GHz (~0.334 cm^{-1}). The comb's

185   center position (line 8) was first coarsely tuned several times between ~6349.15 and ~6349.45 cm$^-$

186   ^{1} (this range corresponds approximately to the FSR of the GSFC). Where the largest intensity

187   reduction on comb line 3 was observed in the coarse tuning, the comb's center position (line 8)

188   was then finely tuned in steps of 0.004 cm^{-1} (0.001 nm), i.e. from 6349.375 to 6349.415 cm^{-1}. For

189   a comb center position at 6349.407 cm^{-1} (line 8) the best overlap between comb line 3 (at

190   6347.7487 cm^{-1}) and comb line 9 (at 6349.7532 cm^{-1}) with absorption features of H_2S was

191   obtained;

192

Fig. 3 The thick black trace is a small spectral segment of the H_2S reference spectrum in Fig. 2 which has been scaled at 6350.71 cm^{-1} to the HITRAN absorption cross-sections (=blue solid dots) for a spectral resolution of 0.08 cm^{-1} (bold axis title, right axis). The thin black trace shows 18 comb lines of the GSFC laser (relative intensity; second title on the right axis). The red trace (left axis) shows the absorption coefficient measured on the 18 comb lines for a center position of the GSFC at 6349.407 cm^{-1} and a comb line spacing of 10 GHz. The red vertical arrows indicate comb lines which overlap significantly with H_2S absorption features at 6347.74, 6349.74, and 6352.74 cm^{-1}.

[#2] Note that using the same FT-spectrometer for FT-IBBCEAS and comb experiments has however the advantage potential wavenumber calibration discrepancies are essentially eliminated.

199

200   Fig. 3 illustrates the situation. The thick black trace in Fig. 3 is a small spectral segment of the H_2S

201   reference spectrum in Fig. 2, which has been scaled at 6350.71 cm^{-1} ($v_1+v_2+v_3$; $4_{22}-3_{21}$) to the

202   HITRAN absorption cross-sections represented by the blue solid dots. The HITRAN cross-section

203   have been evaluated for a spectral resolution of 0.08 cm^{-1} and are only shown for the strongest

204   lines in this spectral region. The cross-section values are shown on the right axis (bold axis title).

205   The thin black trace shows the relative intensity of 18 comb lines of the GSFC, only the position

206   of the comb lines is of relevance here. The red trace (left axis) shows the absorption coefficient

207   measured on the 18 comb lines (discussed below) when the comb line spacing (FSR) was 10 GHz

208   and the center position of the GSFC (line 8) was at 6349.407 cm^{-1}. As mentioned above, for these

209   conditions comb lines 3 and 9 overlap well with H_2S absorption features at 6347.7487 cm^{-1}

210   ($v_1+v_2+v_3$; $5_{24}-4_{23}$) and 6349.7532 cm^{-1} ($v_1+v_2+v_3$; $7_{17}-6_{06}$), respectively. Comb line 18 also

211   overlaps significantly with an absorption feature at 6352.74 cm^{-1} ($v_1+v_2+v_3$; $8_{27}-8_{08}$); these three

212   lines are marked with red vertical arrows in Fig. 3.

213   The spectral separation between the peak absorptions at comb line 3 (at 6347.7487 cm^{-1}) and comb

214   line 9 (at 6349.7532 cm^{-1}) is 2.00451 cm^{-1}, which is slightly larger than 6*FSR = 2.00133 cm^{-1} of

215   the comb. This leaves a potential discrepancy of 0.0032 cm^{-1}, which is smaller than the smallest

216   tuning step size of 0.004 cm^{-1} of the comb's center and ca. 3 times smaller than the expected

217   FWHM of the H_2S absorption lines at the corresponding wavelengths. The discrepancy was within

218   the measurement accuracy of the setup. Nevertheless, assuming the HITRAN line positions to be

219   correct within 0.001 cm^{-1}, a comb FSR of 0.334085 cm^{-1} (15.87 MHz larger than the 10 GHz used)

220   would have been optimum for matching comb lines 3 and 9 with H_2S absorption lines.

221   In comparison, the spectral separation between the peak absorptions at comb line 3 (at 6347.7487

222   cm^{-1}) and comb line 18 (at 6352.7623 cm^{-1}) is 5.0136 cm^{-1}, which is slightly larger than 15*FSR

223   = 5.0033 cm^{-1} of the comb. The discrepancy of 0.0103 cm^{-1} is more significant than that for lines

224   3 and 9. It corresponds to approximately the HWHM of the expected Voigt profile and is thus in

225   agreement with the observation in Fig. 3, i.e. comb line 18 was not exactly positioned in the

226   absorption line center. In conclusion, the position match of comb line 3, 9 and 18 with H_2S

227   absorption lines will never reach the theoretical optimum. The strongest absorption line at

228   ~6351.08 cm^{-1} was unfortunately not overlapping well with comb line 13 (see Fig. 3) for the given

229   center position of the comb and other multiple matching were also not easily attained.

230   We arbitrarily used line 8 of the comb to define the comb's center position, since this line

231   also served as a good reference point for the intensity measurement, I_0, without the sample. In the

232   optimum comb position (at 6349.407 cm^{-1}, see Fig. 3) line 8 does not overlap with any H$_2$S

233   absorption feature, and its peak intensity can be used as "reference intensity", I_0^{ref}, for all other

234   comb lines. Prior to measurements with H$_2$S the spectrum of the comb transmitted by an empty

235   cavity (evacuated at ~0.1 mbar) was extensively measured and averaged. From this reference

236   measurement intensity ratios r_k for each comb line k and center comb line 8 can be calculated;

237    $r_k = I_{0,k}^{\text{ref}} / I_{0,8}^{\text{ref}}$. For a measurement with H$_2$S at first the cavity transmission intensities I_k were

238   stability corrected by dividing through the intensities recorded simultaneously by the OSA. Then

239   the ratio r_k was used to evaluate I_0 on a line that matches a H$_2$S absorption by multiplying r_k by

240   the peak intensity of comb line 8; $I_{0,k} = r_k I_{0,8}$. The absorption coefficient α_k on a matching comb

241   line k can then be calculated from [27, 29]:

242
$$\alpha_k = \frac{1-R}{d}\left(\frac{r_k I_{0,8}}{I_k} - 1\right) \tag{1}$$

243   The absorption coefficients for all α_k in Fig. 3 (red trace, left axis) were calculated using eq. (1).

244   For   the   two   most   relevant   lines   3   and   9   absorption   coefficients

245    $\alpha_3(6347.7487\,\text{cm}^{-1}) = 2.93 \times 10^{-5}\,\text{cm}^{-1}$ and $\alpha_9(6349.7532\,\text{cm}^{-1}) = 1.06 \times 10^{-5}\,\text{cm}^{-1}$ were

246   determined (using $R = 0.993 \pm 0.001$ and $d = 66$ cm). Since the H$_2$S absorption cross-section,

247    $\sigma_3(6347.7487\,\text{cm}^{-1}) = 1.17 \times 10^{-21}\,\text{cm}^2$ and $\sigma_9(6349.7532\,\text{cm}^{-1}) = 4.91 \times 10^{-22}\,\text{cm}^2$ are known

248   from the HITRAN database (converted to instrument resolution, blue dots in Fig. 3), the number

249   density, $n = \alpha_k(\tilde{\nu})/\sigma_k(\tilde{\nu})$, can be calculated. For absorption features on comb lines 3 and 9 we

250   found $n_3 = 2.50 \times 10^{16}$ cm^{-3} and $n_9 = 2.16 \times 10^{16}$ cm^{-3}, corresponding to a discrepancy of the number

251   density of ~13.6%. There are several reasons for this discrepancy: (i) The H$_2$S cross-sections in

252   the HITRAN database have a reported uncertainty of 10% [30] which on two different lines could

253   lead to a max error of 20%. (ii) Even though for this measurement the matching of the comb lines

254   to the maximum of the absorption features on line 3 and 9 was satisfactory, tuning instabilities of

255   the GSFC may cause the comb lines to be not exactly at the maximum of the absorption feature

256   leading to an uncertainty in the expected relative absorption signals. When the GSFC was tuned

257   in between measurements the reproducibility of the number densities on the different absorption

258   lines is decreased due to this effect. The reason is that signal optimization is done at a spectral

259   resolution of only 0.08 cm^{-1} (limited by the FTS). This impinges on the overall error of the

260   measured number densities as further discussed in section 3.2. (iii) The comb intensity was

261   recorded for ~4 hours continuously and the absolute upper limit of the observed intensity

262   fluctuations was found to be ≈3.3%. Systematic uncertainties that may impinge on the absolute

263   value of the number density are the measured value of the mirror reflectivity (0.1%) and the length

264   of the cavity (0.3%), which are considered negligible in comparison to the uncertainties listed

265   above.

266   The averaged number density of 2.33×10^{16} cm^{-3} in this measurement corresponds to 0.92 ppTv.

267   This mixing ratio, calculated from the absorption of sample inside the cavity, was a factor of ~35

268   lower than that initially expected from the partial pressure measured upon sample preparation. For

269   the preparation of H_2S/air gas mixtures a vacuum line with a mixing volume of ~10 dm^3 made of

270   Pyrex glass was set up inside a fume hood because of the hazardous nature of H_2S. For the α_k

271   measurement in Fig. 3 mixtures of H_2S in air were prepared at a ratio of 6:4 at room temperature

272   (assuming no H_2S losses, see below), i.e. the mixing volume was first filled with H_2S at ~400 mbar

273   and then air at a partial pressure of ~600 mbar was added. The mixture was collected for transfer

274   to the cavity setup (Fig. 1) in a small detachable Pyrex glass tube which was connected on one side

275   of the vacuum line via a Teflon valve. The volume of this "transport tube" was ~82 cm^3. As the

276   cavity volume was 998 cm^3 the partial pressures of air and H_2S in the cavity were expected to be

277   49.3 mbar and 32.9 mbar, respectively (provided there are no losses of H_2S when filling the transfer

278   volume). The latter pressure value corresponds to a mixing ratio of 32.4 ppTv under standard

279   conditions (1 atm, 296 K), which is ca. 35 times larger than the amount of H_2S found in the

280   absorption experiment (see above). The reason for this difference is the significant sample loss *in*

281   *the mixing chamber* and transfer volume, as both consisted of Pyrex glass causing inherently large

282   wall losses. Due to efficient chemisorption at metal ion sites in the glass the wall losses in the

283   mixing and transport volume are far from negligible. The fractional throughput of H_2S through a

284   Pyrex glass enclosure is known to be approximately 3% [38], corresponding to losses of a factor

285   ~33 in agreement with the loss factor found in the absorption experiment. Although the data in

286   Ref. [38] are not universal for arbitrary experimental conditions, the low fractional throughput of

287   Pyrex indicates that much less H_2S was collected in the transfer volume. Note that the filling

288   pressure was not measured in the transfer volume itself, but at a distance from it in the larger

289   mixing volume, which was essentially filled with a large excess of air. After the transfer of the

290   sample to the GSFC setup the pressure was measure in the cavity again.

291   To systematically study the effect of losses in the transfer of gas mixtures from the mixing volume

292   to the cavity, the absorption coefficients were determined on laser lines 3 and 9 for five different

293   H_2S concentrations. For these measurements the mixing volume was initially filled with different

294   partial pressures of H_2S between 100 and 500 mbar, then filled up with air to 1000 mbar, and

295   finally transferred to the cavity in the transfer volume. The absorption coefficients on line 3 and 9

296   had an overall uncertainty of $\Delta_{max} < 25\%$ (see Table 1; this error is not to be confused with the

297   difference (discrepancy) in the number densities based on measurements on comb line 3 and 9).

298   The maximal uncertainty of 25% is associated with the reproducibility of the measured absorption

299   coefficient per comb line. For each partial pressure of H_2S the absorption coefficient was measured

300   3-4 times. Between each measurement the GSFC was finely tuned to optimize the signal and to

301   obtain an uncertainty in the reproducibility for a given H_2S concentration, which was evaluated

302   based on a student's t-distribution. Apart from contributions to Δ_{max} that are associated with the

303   uncertainty of the H_2S cross-sections in HITRAN (10%), the optimum position of the comb lines

304   with respect to the absorption maximum was difficult to establish from measurement to

305   measurement as a detection resolution of 0.08 cm^{-1} was used for signal optimization. This

306   resolution is larger than the FWHM of the absorption line at the measurement conditions (~0.021

307   cm^{-1}) and much larger than the comb line width (~10^{-5} cm^{-1}). The accuracy therefore relied strongly

308   the tuning stability of the GSFC, causing a fluctuation in the absorption coefficient and a

309   discrepancy in the relative absorption coefficients measured on line 3 and 9. The 3σ standard

310   deviation of the absorption coefficient on lines that were not matched perfectly with H_2S

311   absorption features was $\approx 3.6 \times 10^{-6}$ cm^{-1}. This value of the minimum absorption coefficient in an

312   integration time of 120 s corresponds to ≈ 680 ppmv, which can be taken as a conservative (upper)

313   limit of detection (LOD) for this approach, because some of the laser lines always overlap to a

314   certain extent with H_2S absorptions, all of which were taken into account in the above stated 3σ

315   LOD. From the H_2S absorption measurements the number densities in the cavity was again

316   estimated based on HITRAN cross-sections, which were systematically (expectedly) smaller than

317   those estimated from the pressure in the mixing volume due to the losses of H_2S in the transfer

318   process. An expected loss factor of ca. 33 (averaged) was found for comb line 9, while the loss

319   factor appeared to be larger (average ~50) for line 3. This difference corroborates that the comb

320   lines 3 and 9 were not equally well matched to the maximum of a H_2S absorption line. While line

321   9 was probably near the maximum of the absorption feature (owing to the smaller loss factor), line

322   3 was positioned off the center of the H_2S absorption line. Within our spectral resolution of only

323   0.08 cm^{-1} the exact position cannot be independently verified. The fact that the ratio of loss factors

324   is approximately constant for all concentrations indicates that the approach is reproducible within

325   the above stated limits, i.e. the laser position and mode structure enabling the light to be transmitted

326   by the cavity is sufficiently stable in the current approach. The data are summarized in Table 1 and

327   graphically represented in Fig. 4.

328
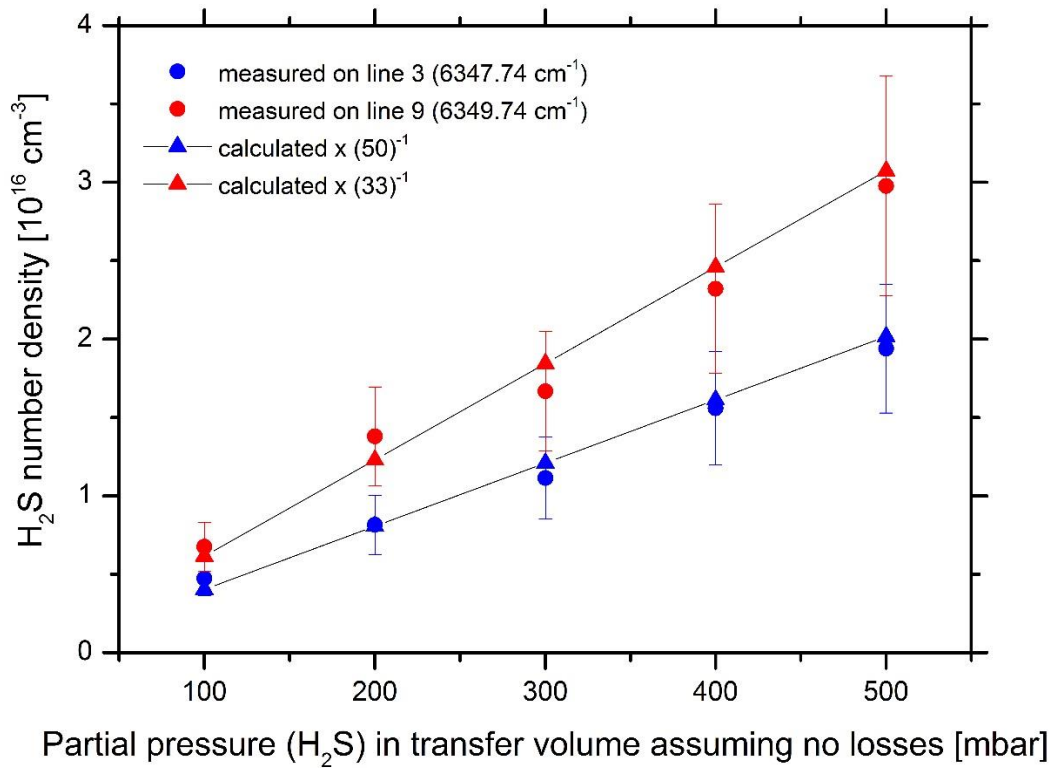
329   **Fig. 4** H_2S number density in the cavity as measured from the absorption coefficient on comb line 3 (blue circles) and
330   line 9 (red circles) vs the alleged partial pressure of H_2S in the mixing volume. The triangular symbols represent the
331   number densities derived from the partial pressures on the horizontal axis, divided by a loss factor of 50 (blue) and 33
332   (red). They can then be compared with the number densities from the absorption measurement. Error bars refer to the
333   uncertainties stated in column 4 of Table 1.

334 **Table 1** Summary of measurement parameter concerning concentration dependent measurements. Values in Column
335 4 vs column 1 are shown in Fig. 4 (cirlces). Col 1: Presumed H_2S partial pressure in 10 dm^3 mixing volume without
336 losses, in [mbar], measured with absolute pressure gauge. Col 2: Anticipated number density in the 1 dm^3 cavity based
337 on pressure in Col 1 and a 82 cm^3 transfer volume, assuming no losses. Col 3: Measured absorption coefficient on line
338 3 and 9. The reproducibility error is 25%. Col 4: Corresponding abs. cross-section from HITRAN database on line 3
339 and 9. Col 5: Number densities following from values in Col 3 and 4. The error in col 3 is explicitly stated here per
340 value (<25%). Col 6: Ratio of the anticipated number density (if there are no losses, Col 2) and the measured number
341 density from the absorption (Col 5). The values corresponds to the approximate loss factor of H_2S in the transfer
342 process from the mixing volume to the cavity. As a factor of ca. 33 is expected from ref [38]; the higher value on line
343 3 indicates that the comb line was not exactly matched to the center (i.e. the maximum) of the H_2S absorption feature.

Pressure [mbar]	Number density [10^{17} cm^{-3}]	Absorption coefficient [10^{-6} cm^{-1}]		Absorption cross-section [10^{-22} cm^2]		Number density [10^{13} cm^{-3}] (ppmv)		Number density ratio – loss factor –	
in mixing volume	calculated from pressure	Line 3	Line 9	Line 3	Line 9	Line 3	Line 9	Line 3	Line 9
		$\Delta_{max} < 25\%$		From HITRAN (uncertainty 10%)		Measured ($\Delta_{max} < 25\%$)		Avg: 50	Avg: 33
100	2.01	5.6	3.3	11.76	4.91	470 ± 100	680 ± 160	43	30
200	4.02	9.6	6.8	11.76	4.91	820 ± 190	1380 ± 320	49	29
300	6.03	13.1	8.2	11.76	4.91	1110 ± 260	1670 ± 380	54	36
400	8.04	18.3	11.4	11.76	4.91	1560 ± 360	2320 ± 530	52	35
500	10.05	22.8	14.6	11.76	4.91	1940 ± 450	2980 ± 680	52	34

344

345 Fig. 4 shows, on the horizontal axis, the partial pressure of H_2S as measured in the mixing volume.
346 On the vertical axis the number densities inside the cavity are shown (circular symbols). They
347 were determined from the absorption coefficient measured on line 3 (blue data points) and line 9
348 (red data points) for the respective mixing partial pressures. The error bars refer to the circular
349 symbols. Additionally displayed are the number densities (triangular symbols, straight black line,
350 no error bars) as they would be expected from the partial pressures, divided by the average loss
351 factor for H_2S for the corresponding line (50 for line 3 and 33 for line 9; cf. Table 1). Fig. 4
352 illustrates the consistency of Table 1 for measurement at different concentrations.

353 The first value in Fig. 4 (100 mbar) is essentially the detection limit. The lower explosion limit
354 (LEL) of H_2S in air is ~4% while the upper explosion limit (UEL) is ~44% [39]. Since the LOD
355 of ~0.7 per mille by volume is significantly smaller than the lower explosion limit (LEL) [39], the
356 GSFC measurements presented here are well sufficient to detect H_2S at its LEL even in the near
357 infrared.

358 Finally, an attempt was made to corroborate our results in Figs. 3 & 4 through the measurement of
359 a high resolution line spectrum, by recording absorption coefficients on line 3 while stepping the

360   center of the GSFC over the optimum position at 6349.407 cm^{-1} (line 8 in Fig. 3) in steps of 0.004

361   cm^{-1}. The problem with this experimental line width test was that all absorption measurements

362   were taken with a resolution of 0.08 cm^{-1}, and the true position of the laser with respect to the line

363   center of the absorption line at 6347.74 cm^{-1} (line 3) could not be determined with sufficient

364   accuracy. The test measurement relied solely on the tuning stability of master laser. Even though

365   the spectrum of the line at 6347.74 cm^{-1} could be recorded by tuning the GSFC, the FWHM was

366   ca. half the size of the anticipated Voigt FWHM (0.021 cm^{-1}) according to the estimated pressure

367   and Doppler broadening, see above. This discrepancy is likely to be a consequence of the electronic

368   tuning stability and potential small drifts of the GSFC. The stability was investigated by

369   independently tuning to the GSFC center position to the maximum absorption signal many times

370   in the context of the I_0 measurements. The absolute laser position, as solely determined from the

371   tuning voltage, could be reproduced within 0.017 cm^{-1}, which is 20% smaller than the anticipated

372   FWHM of the expected H_2S absorption line. The tuning to the maximum position is uncertain

373   within that limit, explaining the different loss factors found for the laser comb lines 3 and 9.

374   **4.   Conclusions and outlook**

375   Two comb lines (3 and 9) were matched to absorption lines of H_2S in the near infrared L-band

376   without locking the laser to the cavity mode structure. Without locking the laser line, the overlap

377   of the laser with the absorption features was accurate and stable to within ≈80% of the FWHM of

378   the absorption line. From the non-resonant comb lines, an rms noise equivalent absorption for this

379   approach of approximately 3.9×10^{-5} cm^{-1} $Hz^{-1/2}$ was found, which corresponds to a detection limit

380   of ca. 700 ppmv of H_2S in 120 s. This sensitivity is well below the lower explosion limit of H_2S

381   of 4% and was achieved with a very modest finesse (~450) cavity.

382   Future work will focus on making the setup more compact by using custom-designed integrated

383   combs and improving the detection resolution through a dual comb approach. Alternative coupling

384   scheme of the laser to the cavity will be looked into and the detection cell is to be developed into

385   a flow cell. Other spectral regions are to be targeted.

386

387

388

Acknowledgement

References

[1]   J. Ye, S.T. Cundiff (Eds.), *Femtosecond Optical Frequency Comb: Principle, Operation, and Applications*, (Kluwer Academic Publishers/Springer, Norwell MA, 2005)

[2]   T. W. Hänsch, Nobel lecture: Passion for precision. Rev. Mod. Phys. **78,** 1297–1309 (2006).

[3]   J. L. Hall, Nobel lecture: Defining and measuring optical frequencies. Rev. Mod. Phys. **78,** 1279–1295 (2006)

[4]   S.A. Diddams, The evolving optical frequency comb. J. Opt. Soc. Am. B **27,** B51–B62 (2010)

[5]   N.R. Newbury, Searching for applications with a fine-tooth comb. Nat. Photonics **5,** 186–188 (2011)

[6]   T.W. Hänsch, N. Picqué, Laser spectroscopy and frequency combs. J. Phys. Conference Series **467,** 012001 (2013)

[7]   F. Adler, M.J. Thorpe, K.C. Cossel, J. Ye, Cavity-enhanced direct frequency comb spectroscopy: Technology and applications. Annu. Rev. Anal. Chem. **3,** 175–205 (2010)

[8]   S.A. Diddams, L. Hollberg, V. Mbele, Molecular fingerprinting with the resolved modes of a femtosecond laser frequency comb. Nature **445,** 627–630 (2007)

[9]   L. Nugent-Glandorf, T. Neely, F. Adler, A.J. Fleisher, K.C. Cossel, B. Bjork, T. Dinneen, J. Ye, S.A. Diddams, Mid-infrared virtually imaged phased array spectrometer for rapid and broadband trace gas detection. Opt. Lett. **37,** 3285–3287 (2012)

[10] C. Gohle, B. Stein, A. Schliesser, T. Udem, T.W. Hänsch, Frequency comb vernier spectroscopy for broadband, high-resolution, high-sensitivity absorption and dispersion spectra. Phys. Rev. Lett. **99,** 263902 (2007)

[11] R. Grilli, G. Méjean, C. Abd Alrahman, I. Ventrillard, S. Kassi, D. Romanini, Cavity-enhanced multiplexed comb spectroscopy down to the photon shot noise. Phys. Rev. A **85,** 051804 (2012)

[12] J. Mandon, G. Guelachvili, N. Picqué, Fourier transform spectroscopy with a laser frequency comb. Nat. Photonics **3,** 99–102 (2009)

[13] F. Adler, P. Masłowski, A. Foltynowicz, K. C. Cossel, T. C. Briles, I. Hartl, J. Ye, Mid-infrared Fourier transform spectroscopy with a broadband frequency comb. Opt. Express **18,** 21861–21872 (2010)

428 [14] B. Bernhardt, A. Ozawa, P. Jacquet, M. Jacquey, Y. Kobayashi, T. Udem, R. Holzwarth,
429   G. Guelachvili, T. W. Hänsch, N. Picqué, Cavity-enhanced dual-comb spectroscopy.
430   Nature Photonics **4**, 55–57 (2010)
431 [15] M. Zeitouny, P. Balling, P. Křen, P. Mašika, R.C. Horsten, S.T. Persijn, H.P. Urbach, N.
432   Bhattacharya, Multi-correlation Fourier transform spectroscopy with the resolved modes of
433   a frequency comb laser. Ann. Phys. **525,** 437–442 (2013)
434 [16] A. Khodabakhsh, A.C. Johansson, A. Foltynowicz, Noise-immune cavity-enhanced optical
435   frequency comb spectroscopy: a sensitive technique for high-resolution broadband
436   molecular detection. Appl. Phys. B **119,** 87–96 (2015)
437 [17] A.J. Fleisher, D.A. Long, Z.D. Reed, J.T. Hodges, D.F. Plusquellic, Coherent cavity-
438   enhanced dual-comb spectroscopy. Opt. Express **24,** 10424–10434 (2016)
439 [18] I. Coddington, N. Newbury, W. Swann, Dual-comb spectroscopy. Optica **3,** 414–426
440   (2016)
441 [19] T. Gherman, D. Romanini, Mode–locked cavity–enhanced absorption spectroscopy. Opt.
442   Express **10,** 1033–1042 (2002)
443 [20] A. Foltynowicz, P. Masłowski, A.J. Fleisher, B.J. Bjork, J. Ye, Cavity-enhanced optical
444   frequency comb spectroscopy in the mid-infrared application to trace detection of
445   hydrogen peroxide. Appl. Phys. B **110,** 163–175 (2013)
446 [21] M. J. Thorpe, J. Ye, Cavity-enhanced direct frequency comb spectroscopy, Appl. Phys. B
447   **91,** 397–414 (2008)
448 [22] P. M. Anandarajah, R. Maher, Y. Xu, S. Latkowski, J. O'Carroll, S.G. Murdoch, R. Phelan,
449   J. O'Gorman, L.P. Barry, Generation of coherent multicarrier signals by gain switching of
450   discrete mode lasers. IEEE Photonics J. **3,** 112 (2011)
451 [23] P. Anandarajah, R. Zhou, R. Maher, M.D. Guitérrez-Pascual, F. Smyth, V. Vujicic, L.P.
452   Barry, Flexible optical comb source for super channel systems. Optical Fiber
453   Communication Conference, Proceedings Paper# OTh3I.8, Anaheim CA, USA (2013)
454 [24] M.D. Guitérrez, J. Braddell, F. Smyth, L. P. Barry, Monolithically integrated 1´4 comb de-
455   multiplexer based on injection locking. 18th European Conference on Integrated Optics,
456   Proceedings Paper# ECIO-p37, Warsaw, Poland (2016)
457 [25] B. Jerez, P. Martín-Mateos, E. Prior, C. de Dios, P. Acedo, Dual optical frequency comb
458   architecture with capabilities from visible to mid-infrared. Opt. Express **24,** 14986–14994
459   (2016)
460 [26] W. Chen, A.A. Kosterev, F.K. Tittel, X. Gao, W. Zhao, H_2S trace concentration
461   measurements using off-axis integrated cavity output spectroscopy in the near-infrared.
462   Appl. Phys. B **90,** 311–315 (2008)
463 [27] S.E. Fiedler, A. Hese, A.A. Ruth, Incoherent broadband cavity-enhanced absorption
464   spectroscopy. Chem. Phys. Lett. **371,** 284–294 (2003)
465 [28] A.A. Ruth, J. Orphal, S.E. Fiedler, Cavity enhanced Fourier transform absorption
466   spectroscopy using an incoherent broadband light source. Appl. Opt. **46,** 3611–3616 (2007)
467 [29] J. Orphal, A.A. Ruth, High-resolution Fourier-transform cavity-enhanced absorption
468   spectroscopy in the near-infrared using an incoherent broad-band light source. Opt. Express
469   **16,** 19232–19243 (2008)
470 [30] D.M. O'Leary, A.A. Ruth, S. Dixneuf, J. Orphal, R. Varma, The near infrared cavity-
471   enhanced absorption spectrum of methylcyanide. J. Quant. Spectr. Rad. Trans. **113,** 1138–
472   1147 (2012)

473 [31] R. Raghunandan, A. Perrin, A.A. Ruth, J. Orphal, First analysis of the $2\nu_1+3\nu_3$ band of NO_2
474   around 7192 cm^{-1}. J. Mol. Spectrosc. **297,** 4–10 (2014)
475 [32] S. Chandran, R. Varma, Near infrared cavity enhanced absorption spectra of
476   atmospherically relevant ether-1,4-dioxane. Spectrochim. Acta A: Mol. Biomol. Spectr. **153**,
477   704–708 (2016)
478 [33] L.S. Rothmana, I.E. Gordon, Y. Babikov, A. Barbe, D. Chris Benner, P.F. Bernath, M. Birk,
479   L.Bizzocchi, V.Boudon, L.R. Browni, A. Campargue, K. Chance, E.A. Cohen, L.H.Coudert,
480   V.M. Devi, B.J.Drouin, A. Fayt, J.-M. Flaud, R.R. Gamachem, J.J. Harrison, J.-M.
481   Hartmann, C. Hill, J.T. Hodges, D. Jacquemart, A. Jolly, J. Lamouroux, R.J. LeRoy, G. Li,
482   D.A. Long, O.M. Lyulin, C.J. Mackie, S.T. Massie, S. Mikhailenko, H.S.P. Müller, O.V.
483   Naumenko, A.V. Nikitin, J. Orphal, V. Perevalov, A. Perrin, E.R. Polovtseva, C. Richard,
484   M.A.H. Smith, E. Starikova, K. Sung, S. Tashkun, J.Tennyson, G.C. Toon, V.G. Tyuterev,
485   G. Wagner, The HITRAN 2012 molecular spectroscopic database. J. Quant. Spectr. Rad.
486   Trans. **130,** 4–50 (2013)
487 [34] S.W. Sharpe, T.J. Johnson, R.L. Sams, P.M. Chu, G.C. Rhoderick, P.A. Johnson, Gas-phase
488   databases for quantitative infrared spectroscopy. Appl. Spectrosc. **58,** 1452–1461 (2004)
489 [35] O.N. Ulenikov, A.-W. Liu, E.S. Bekhtereva, O.V. Gromova, L.-Y. Hao, S.-M. Hu, High-
490   resolution Fourier transform spectrum of H_2S in the region of the second hexade. J. Mol.
491   Spectrosc. **234,** 270–278 (2005)
492 [36] G. Modugno, C. Corsi, M. Gabrysch, M. Inguscio, Detection of H_2S at the ppm level using
493   a telecommunication diode laser. Opt. Com. **145,** 76–80 (1998)
494 [37] J.J. Olivero, R.L. Longbothum, Empirical fits to the Voigt line width: A brief review. J.
495   Quant. Spectr. Rad. Trans. **17,** 233–236 (1977)
496 [38] W.C. Kuster, P.D. Goldan, Quantitation of the losses of aqueous sulfur compounds to
497   enclosure wall, Env. Sci. Technol. **21,** 810–815 (1987)
498 [39] M.G. Zabetacis, Flammability characteristics of combustible gases and vapors, Bulletin 627,
499   US Department of the Interior, Bureau of Mines (1965)